Journal of Catalysis **199,** 155–161 (2001)
doi:10.1006/jcat.2001.3172, available online at http://www.idealibrary.com on IDEAL®

Active Carbon Supported Mo–K Catalysts Used for Alcohol Synthesis

Zhong-rui Li,* Yi-lu Fu,*,[1] Ming Jiang,* Tian-duo Hu,† Tao Liu,† and Ya-ning Xie†

*Department of Chemical Physics, University of Science and Technology of China, Hefei 230026, People's Republic of China; and †Institute of High Energy Physics, Chinese Academy of Science, Beijing 100039, People's Republic of China

Received January 12, 2000; revised January 9, 2001; accepted January 12, 2001; published online March 21, 2001

The structure of oxidic and sulfided Mo catalysts supported on activated carbon was studied by means of X-ray diffraction (XRD), laser Raman spectroscopy (LRS), and extended X-ray absorption fine structure (EXAFS). The activity for mixed alcohol synthesis was also investigated. In oxidic state, the Mo phase on the sample with low Mo loading is mainly present as MoO_2, due to the migration of the potassium anions into micropores of activated carbon and the reducing nature of activated carbon at a high preparation temperature. As the Mo loading increases, the interaction between potassium and molybdenum is enhanced. At the MoO_3 loading of 72 wt%, Mo mainly exists in the form of $K_2Mo_2O_7$ species. After sulfidation, the O–S substitution takes place; the Mo sulfide phase is highly dispersed as tiny three-dimensional particles at higher loading. Indeed, the results of XRD, LRS, and EXAFS demonstrate that MoS_2 is the major phase present after sulfidation. The higher catalytic activity for Mo–K/AC compared to Mo–K/Al_2O_3 is explained by the difference in the structure of sulfide phase and in the interaction between these phases and the respective supports.

Key Words: **molybdenum-based catalysis; activated carbon support; alcohol synthesis; structure.**

1. INTRODUCTION

The worldwide trend toward unleaded gasoline demands a growing need for high octane blending components. Mixtures of methanol and higher alcohols ($C_{2+}OH$), also called mixed alcohols, have the potential for providing a gasoline-blending stock superior to that of straight-run methanol or ethanol (1). The development of catalysts and processes by which such alcohol mixtures can be synthesized directly from syngas is a subject of both academic and industrial interest. In this aspect, molybdenum-based catalysts are of a special interest because of their resistance to sulfur poisoning (a difficult problem with metallic catalysts) (2), particularly also claims by several U.S. patents (3–6).

The activity and selectivity for mixed alcohols formation over Mo catalysts were significantly affected by the supports, the additive such as alkali metal salts, and the reaction conditions (7). Catalysts based on activated carbon (AC) hold several advantages when comparing them with silica- and alumina-based catalysts. Interaction between the support and the active material is limited to a large extent by the inertness of the graphitic surface. In many cases, this can result in an optimized utilization of the metals applied. An example is the hydrodesulfurization (HDS) of the thiophene by supported cobalt molybdenum catalysts. Catalysts based on activated carbon display a higher (2–3 times) activity per unit weight metal compared to Co–Mo/Al_2O_3 catalysts (8). The thermostability of activated carbon in inert environments at elevated temperatures is considerably higher than that of SiO_2 and Al_2O_3, up to 1700 K no significant sintering of the support is observed (9). Another benefit of using activated carbon as a support is its stability in caustic and acidic solutions.

In view of the intriguing properties of carbon-supported HDS catalysts, many authors (9–11) had attempted to explain the observed activity difference between activated carbon-supported (Mo/AC) and alumina-supported (Mo/Al_2O_3) Mo sulfide catalysts. The salient conclusion was that the observed superior activity of the Mo/AC catalysis, especially at low Mo loadings, should be attributed to the presence of a Mo sulfide phase at the carbon surface which has both a higher fraction of catalytically active surface area and a higher HDS activity per active site compared with the Mo sulfide phase present on the Al_2O_3 support surface. This strongly suggests that at low Mo loadings the Mo sulfide phases present on activated carbon and alumina supports are not identical. Furthermore, it was demonstrated (9, 10) that at high Mo loadings the properties of the Mo sulfide phase present on alumina tended toward those of the Mo/AC system, emphasizing that at very high Mo loadings the carbon- and alumina-supported sulfide phase are essentially the same.

Mo-based catalysts used for alcohol synthesis were evolved from that for HDS by appropriate modification. However, so far the support effects of activated carbon and alumina are still not clear on alcohol synthesis from CO hydrogenation. The objective of our work has been to investigate Mo–K catalysts supported on activated carbon

[1] To whom correspondence should be addressed.

0021-9517/01 $35.00

and alumina in an attempt to obtain more highly dispersed and more active catalysts. In this paper, we report our findings that the activated carbon supported Mo–K catalysts are active in the synthesis of mixed alcohols. The interaction between the activated carbon and molybdenum components and its effect on sulfidability and dispersion of the supported molybdenum species are elucidated based upon the characterizations using a variety of techniques. The observed activity differences between activated carbon-supported (Mo–K/AC) and alumina-supported (Mo–K/Al_2O_3) Mo sulfide catalysts are discussed by comparing the results with those reported in the literature for Mo–K/Al_2O_3.

2. EXPERIMENTAL

2.1. Sample Preparation

The activated carbon (China Medicine Co.) was ground to 35–60 mesh (425–250 μm) and washed with HNO_3 (1 M) and distilled water several time before use. After washing and drying, the BET surface area is 750 m^2/g, pore volume 0.68 ml/g, total ash beneath 0.1 wt%. The oxidic Mo–K/AC samples were prepared by sequential pore volume impregnation and calcination technique. At the first step, the activated carbon was impregnated with a solution of K_2CO_3, followed by drying and calcining at 573 K. It was further impregnated with $(NH_4)_6Mo_7O_{24} \cdot 4H_2O$ solution by drying at 393 K for 12 h and calcining in a nitrogen flow (purified by passing through a 105 deoxy agent and 5A zeolite) of 40 ml min^{-1} at 773 K for 24 h. The sulfided samples were obtained by heat-treating the oxidic precursors in a flow of mixed CS_2/H_2 gas [obtained by passing H_2 (30 ml min^{-1}) through CS_2 liquid at 273 K] at 673 K for 6 h. The molybdenum content in the samples, expressed as a weight ratio of MoO_3/C, varies from 0.24 to 0.72 and the atomic ratio of K/Mo is 0.8. Catalyst samples were denoted as $MoO_3(x)$-K/AC, where $x =$ wt% MoO_3.

2.2. Characterization Methods

The crystalline phases of the samples were examined by X-ray diffraction (XRD) with Cu $K\alpha$ radiation (0.1542 nm) on a D/MAX-γA rotatory target diffractometer (40 kV and 100 mA). For the measurements, the samples were ground to fine powder and packed into specimen holders.

Laser Raman spectra (LRS) were recorded on a SPEX-1403 spectrometer with a resolution of ± 2 cm^{-1} using the 488.0-nm^{-1} radiation line from a Spectra-Physics-2020 argon laser. The laser beam intensity and the spectrum slit width were 100 mW and 3.5 cm^{-1}, respectively. The samples were pressed into wafers for the measurements.

The spectra of extended X-ray absorption fine structure (EXAFS) were measured at the beamline of 4WIB of Beijing Synchrotron Radiation Facility (BSRF). The storage ring was operated at 2.2 GeV with a typical current of 50 mA. The fixed-exit Si(111) flat double crystal was used as the monochromator. The spectra were recorded in transmission mode with ionization chambers filled with argon. The K-edge of molybdenum atom positioned at 19,999 eV was used for calibration. Data analysis was performed following a standard procedure (12). Phase shifts and backscattering amplitudes extracted from the spectra of $Na_2MoO_4 \cdot 2H_2O$ and MoS_2 standard compounds were used to calculate the structural parameters of the samples.

2.3. Measurements of Catalytic Activity

Mixed alcohol synthesis was performed in a tubular downflow, fixed-bed reactor system. Feed gases were composed of CO (30%), H_2 (60%), and N_2 (10%) and passed through mass flow controllers. The reactor was a stainless tube of 350-mm length and 6-mm inside diameter. It is housed in an electric furnace equipped with a temperature controller. The effluent gas was cooled to 273 K and separated into gas and liquid phases at high pressure. The gaseous products were directly analyzed on a chromatograph through a sampling valve, and the liquid products were collected for a proper period with their volume and weight measured; they were subsequently analyzed on the same chromatograph by injection. CO, CO_2, and H_2 in the gas and H_2O in the liquid products were analyzed on a 2-m TDX-01 column by using a thermal conductivity detector with argon as the carrier gas. The hydrocarbons, alcohols, and other oxygenated compounds were analyzed on a 2-m Porapak Q column by using a hydrogen flame detector with N_2 as the carrier gas. The composition of hydrocarbons was calculated using 1.04% CH_4 as standard gas, while that of the mixed alcohol was calculated directly from the peak areas by using a standard liquid of C_1–C_5 mixed alcohols. Under the present experimental conditions, the thermal conductivity detector could detect only trace amount of CO_2, and thus the activity mentioned below would be referred to as CO_2-free. Note that the formation of methane by reduction of the support is not a problem at the temperatures used to test the catalysts. In the absence of CO, no hydrocarbon products were detected when the catalysts were heated in hydrogen at 673 K.

3. RESULTS

3.1. XRD

The XRD patterns of the oxidic samples are shown in Fig. 1 and indicate several phases as expected. For the low Mo loading samples (MoO_3(24%)–K/AC), on the activated carbon support, Mo mainly exist in the form MoO_2 with d-spacing values of 0.343, 0.243, 0.171, 0.140 nm, with the addition of a tiny amount of $K_xMo_yO_z$ (K–Mo) species ($d = 0.336$, 0.325 nm). This can be interpreted from the preparation technique. The potassium ion is smaller in size than the molybdate ion. Hence, some of the potassium ions

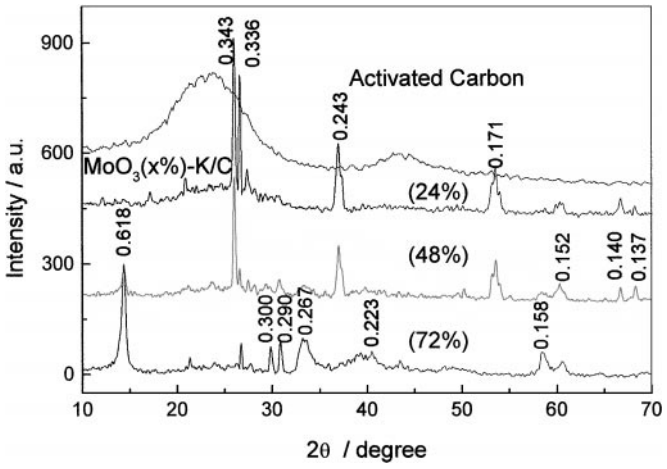

FIG. 1. XRD patterns of oxidic $MoO_3(x\%)$–K/AC samples with different Mo loading.

take precedence of molybdate to migrate into the micropore of the activated carbon. As a result, potassium could not interact fully with molybdenum to form the K–Mo species. In addition, during the decomposition at high preparation temperatures the Mo species were reduced from Mo(VI) to Mo(IV), the activated carbon acting as the reducing agent. With increasing Mo loading, the intensity of MoO_2 peaks decrease dramatically, and the diffraction peaks of $K_2Mo_2O_7$ appear. For the sample with MoO_3 loading of 72%, the MoO_2 diffraction peaks completely disappear, and Mo mainly appears as $K_2Mo_2O_7$ species ($d = 0.618$, 0.330, 0.300, 0.290, 0.267, 0.223, 0.158 nm).

The XRD patterns of sulfided samples are quite different from those of oxidic samples. After sulfidation, the diffraction of the K–Mo–O species observed for the oxidic samples are removed (Fig. 2), and MoS_2 diffraction peaks ($d = 0.609, 0.271, 0.158, 0.153, 0.263, 0.234, 0.219$ nm) appear

TABLE 1

Characteristic Sizes (nm, D_c*) of Catalysts before Reaction

Sample MoO_3 wt%	Oxidic		Sulfided
	MoO_2	$K_2Mo_2O_7$	MoS_2
24	26	—	88
48	23	26	125
72	—	39	143

Note. * $D_c = 0.89\,\lambda/(B\cos\theta)$; λ is the wavelength of Cu $K\alpha$ X-ray radiation; θ denotes the Bragg angle; B is the half-width corrected for $K\alpha$-doublet separation and instrumental broadening.

and increase with the molybdenum loading. This indicates that oxygen in the sample is substituted by sulfur, and the species transforms to three-dimensional MoS_2 crystallites as the molybdenum loading increases. The crystallite sizes, Dc (nm), are calculated from the line width of the diffraction peaks using the Scherrer formula with correction for instrumental line broadening and are listed in Table 1.

3.2. LRS

Raman spectra of the oxidic samples are shown in Fig. 3. For the low Mo-loading sample (i.e., MoO_3(24%)–K/AC), the bands at 830–970 cm^{-1} indicate that there is a tiny amount of octahedrally and tetrahedrally coordinated molybdenum species, and the weak bands at 206, 348, 462 cm^{-1} can be assigned to the different Mo–O vibration modes of MoO_2 (13). With the increase in Mo loading, the Raman spectra take a different look. The intensity of the MoO_2 bands decrease monotonically with the Mo loading, and new bands, which increase with Mo loading, are obviously detected in the Raman spectra of the high Mo-loading samples (i.e., MoO_3(72%)–K/AC). According

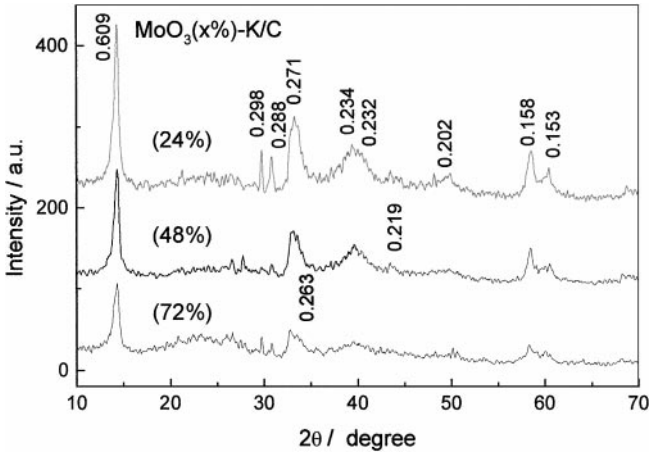

FIG. 2. XRD patterns of sulfided $MoO_3(x\%)$–K/AC samples with different Mo loading.

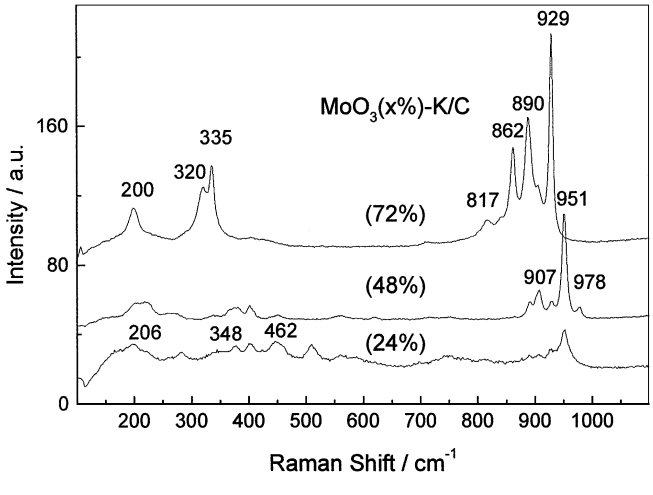

FIG. 3. LRS of oxidc $MoO_3(x\%)$–K/AC samples with different Mo loading.

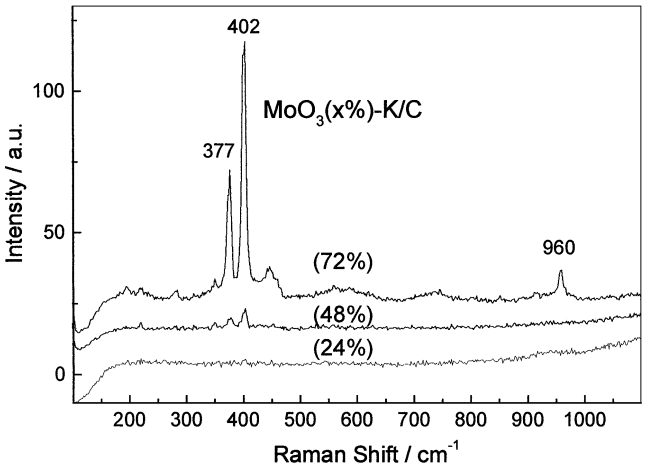

FIG. 4. LRS of sulfided $MoO_3(x\%)$–K/AC samples with different Mo loading.

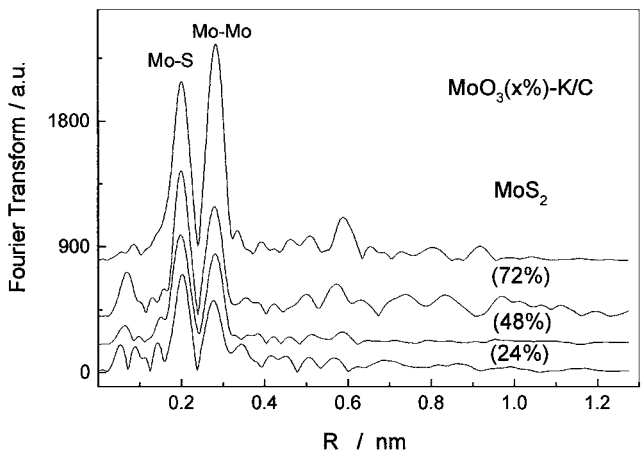

FIG. 5. Fourier transforms of $k^3\chi(k)$ for the crystalline MoS_2 and the sulfided $MoO_3(x\%)$–K/AC samples.

to a study on the Raman vibrations of supported tetrahedrally coordinated molybdenum species (14), the $Mo_2O_7^{2-}$ anion, made from two corner-sharing (MoO_4) tetrahedra, display a Mo–O symmetric stretch at 930 cm^{-1} and a Mo–O bend at 320 and 335 cm^{-1}. The antisymmetric stretching and symmetric bending modes of Mo–O–Mo linkage were observed at 862 and 200 cm^{-1}, respectively. Based on the result of XRD, the new Raman vibrations can be assigned to $K_2Mo_2O_7$ species, which contain the $Mo_2O_7^{2-}$ ion. On the MoO_3(72%)–K/AC sample, only a very weak band at 817 cm^{-1} could be detected (the strongest Raman scattering for MoO_3), which means Mo mainly exists in the form of the $K_2Mo_2O_7$ species.

After sulfidation, the Raman spectra (Fig. 4) of these samples are different from those of oxidic samples. Almost no band could be detected on the low Mo loading samples (such as MoO_3(24%)–K/AC). As the Mo loading increases, the characteristic bands (377 and 402 cm^{-1}) of MoS_2 begin to appear, and no other species are found. The strong MoS_2 peaks demonstrate that Mo(VI) are basically converted into MoS_2 species. This result is consistent with the XRD result. Further increase in Mo loading leads to a significant increase of the intensity of the MoS_2 bands. Moreover, a broad band around 960 cm^{-1} becomes observable at MoO_3 loading of 72 wt%. The broad feature could be ascribed to the surface oxysulfide-molybdenum species, as suggested by Schrader and Cheng (15), and it is associated with the extent of sulfidation of the molybdenum components.

3.3. *EXAFS*

The magnitude of the Fourier transforms ($k^3\chi(k)$, $\Delta k = 17 \sim 151$ nm^{-1}) of the samples together with those of the MoS_2 standard compound are shown in Fig. 5. MoS_2 is of hexagonal structure with one molybdenum atom surrounded by six sulfur atoms at a distance of 0.241 nm and six molybdenum neighbors at 0.316 nm. In the Fourier transforms of the samples (Figs. 5b–5d), mainly two peaks are observed at 0.204 and 0.283 nm. They are located almost at the same positions as those for MoS_2 standard compound (Fig. 5a), indicating that the local structure of the sulfided molybdenum species is similar to that of MoS_2. For the sulfided Mo–K/AC samples, the magnitudes of Fourier transforms of the Mo–S and Mo–Mo coordinations increase with Mo loading and the ratios of the magnitude of Mo–Mo shell to that of the Mo–S shell are also higher. The analysis of Mo–S and Mo–Mo peaks was carried out using inverse Fourier transform followed by a fitting procedure on the isolated EXAFS functions. The structural parameters obtained from the fitting results for the Mo coordination shells are presented in Table 2. For clarity, the crystallographic data, coordination numbers, and distances of the

TABLE 2

Structure Parameters from the Fourier-Filtered Data for the Sulfided Samples

Sample (MoO_3 wt%)	Bond	R/nm	N	$\Delta\sigma^2$ (10^{-6}/nm^2)[a]	ΔE_0/eV[b]
24	Mo–S	0.242	3.03	0	−0.167
	Mo–Mo	0.313	2.01	1	4.21
48	Mo–S	0.241	3.51	0	0.52
	Mo–Mo	0.316	2.49	0	1.60
72	Mo–S	0.241	3.59	1	−1.50
	Mo–Mo	0.314	3.03	0	0.73
MoS_2	Mo–S	0.241	6.0		
	Mo–Mo	0.316	6.0		

[a] Relative Debye–Waller factor of the sample to that of the standard compounds.

[b] Correction of the innerpotentials of the samples based upon those of the crystalline MoS_2.

TABLE 3

Performance of Alcohol Synthesis over Sulfided Mo–K/AC Samples

Sample (MoO_3%)	CO Conv. (%)	Sel. alc. (CO%)	MeOH $C_{2+}OH$	STY[a] (CO mol/kg/h)	STY[a] (CO mol/m^2/h)
24	9.4	36.8	1.01	15.8	0.6
36	11.2	37.5	0.98	19.7	1.1
48	12.8	38.3	0.91	23.1	1.4
60	14.4	40.7	0.83	21.9	1.3
72	16.2	41.2	0.72	20.3	1.2
24[b]	7.2	39.4	0.87	7.4	0.3

Note. Reaction conditions: 603 K, 5.0 MPa, 7200 h^{-1}, $H_2/CO = 2$ (v/v).

[a] STY is expressed as mole of CO reacted into alcohols over per kg or m^2 of MoS_2 in one hour.

[b] Sulfided MoO_3(24%)–K/Al_2O_3 catalyst sample (calcined at 1073 K) (17).

MoS_2 standard compounds, which were used to extract the experimental phase and amplitude functions of the samples, are also collected in Table 2. The errors for the fitted parameters corrected as described by Stern *et al.* (16) are estimated to be 20% in coordination number N, 1% in distance R, 10% in Debye–Waller factor $\Delta\sigma^2$, and 10% in ΔE_0. Since the backscattering amplitudes contain an unknown static and thermal disorder and a damping due to photoelectron losses in the shells, the values of the disorder parameter $\Delta\sigma^2$ reported for the samples are given relative to those for the standard compounds. The small $\Delta\sigma^2$ values for all samples indicate a locally ordered, three-dimensional MoS_2 structure, not like the large patch MoS_2 slabs with higher disorder in the Mo–K/Al_2O_3 samples (17). The coordination number of Mo–Mo often suggests the size of MoS_2, an increase in N_{Mo-Mo} indicating that the particle size of MoS_2 over activated carbon gets larger with increasing Mo loading. This result is also consistent with that of XRD.

3.4. Mixed Alcohol Synthesis

The effects of Mo loading on the activity and selectivity of the carbon monoxide–hydrogen reaction are given in Table 3. Data in Table 3 were obtained under the reaction conditions with optimized temperature of about 603 K. The space-time-yield (STY) is expressed in both specific activities (mole of CO reacted into alcohols over unit area of MoS_2 in hours) and the mole of CO converted into alcohols per kg of MoS_2 per hour. With the increase of Mo loading, the activity for alcohol synthesis expressed as STY is optimized at MoO_3 loading of 48%. The more important point to be mentioned is that the selectivity for alcohol formation (Sel. alc.) increases monotonically and C_{2+} alcohol proportion ($MeOH/C_{2+}OH$) in the product is also improved with increasing Mo loading. For the low Mo-loading sample, $C_1OH/C_{2+}OH$ in product is higher, because of K-first and Mo-last impregnation sequence, which leads to incompletely interaction between Mo and K as mentioned before. The K–Mo interaction enhanced with increase in Mo loading, and $C_1OH/C_{2+}OH$ decrease also. At MoO_3 loading of 72%, $C_1OH/C_{2+}OH$ decreases to 0.72 as much as that over alumina. As literature reported, at high Mo loading, The molybdenum sulfide on activated carbon has the same structure as that on alumina. At the same Mo loading (i.e., MoO_3 24 wt%), The yield (CO mol/kg/h) over activated carbon is much higher than that over alumina, the difference in them is even pronounced at higher Mo loading.

4. DISCUSSION

4.1. Comparison with Other Studies of Mixed Alcohol Synthesis over Activated Carbon-Supported Catalysts

It is necessary to make a comparison of the catalytic activity of our catalysts with those of previous catalytic systems. In Table 4 we listed the activities of our sulfided MoO_3(48%)–K/AC catalyst (D) and those of some similar catalysts in patents. For the reasonable comparison, the data in Table 4 were collected in the reaction under similar reaction conditions, due to the factor of the reaction conditions can significantly affect the activity and selectivity for mixed alcohols formation over Mo-based catalysts (7). Our sulfided MoO_3(48%)–K/AC catalyst is about 50% higher in activity than unsupported sample A. Since we used a high-surface-area activated carbon it is likely that our catalyst had a high dispersion as shown in Table 1. In contrast, unsupported MoS_2 easily aggregated in the reaction process; hence, a small fraction of the unit weight is active.

For the activated carbon supported catalysts, our catalysts have activity similar to those claimed in patents as seen in Table 4. The selectivity of these activated carbon supported catalysts seems to be dependent on the method

TABLE 4

Comparison of the Activities and Selectivities of Sulfided Mo–K Catalysts

Sample	A	B	D	D
Temp. (K)	538	589	538	590
H_2/CO molar ratio	1.04	1.07	1.0	1.0
GHSV (h^{-1})	1200	4200	1200	4200
Pressure (MPa)	10.45	13.89	10.0	14.0
H_2S added (ppm)	0	138	0	0
CO Conver. (C%)	33.1	19.0	45.0	17.6
Sel. alc. (C%)	73.6	75.3	72.8	73.4
$C_1OH/C_{2+}OH$ molar ratio	0.78	1.85	0.79	0.87
STY. alc. (CO mol/kg/h)	6.78	28.9	9.14	26.1

(A) "Comparison A" in U.S. Patent 4,882,360 (1989) (4).
(B) "Example 1c" in U.S. Patent 4,675,344 (1987) (6).
(D) Sulfided MoO_3(48%)–K/AC samples in this work.

of preparation, H_2S concentration in reactant gas, and other factors. For practical points of view, it is very desirable to enhance the C_{2+} alcohols content in product. Cochran *et al.* and Conway *et al.* increase C_{2+} alcohol content by addition of H_2S into the feed for process (5, 6). However, the high H_2S concentration is very deleterious to the reaction system, hence increasing H_2S concentration in synthesis gas is not the right way to raise higher alcohol selectivity. It is interesting that even under the conditions of H_2S free our catalyst shows a higher C_{2+} alcohol formation rate as suggested by the low $C_1OH/C_{2+}OH$ molar ratio. It is likely that the difference is due to different type of active surface rather than surface area.

One important thing we want to mention is that reaction temperatures used in Table 4 are not optimized for our catalysts. Our previous research found that, at proper reaction temperature and CO/H_2 ratio, increasing pressure and space velocity could drastically improve the activity and selectivity for sulfided Mo–K catalysts. For example, our laboratory succeeded in preparing a new kind of sulfided K–Mo/Al_2O_3 catalyst which showed relatively high activity and selectivity for mixed alcohols synthesis. Under the reaction condition of 658 K, 14.0 MPa, and 11000 h^{-1}, the alcohol space–time yield (STY) was up to 31.7 CO mol/MoS_2 kg/h (12.8 CO mol/MoS_2 m^2/h) and alcohol selectivity was 82% (20). Activated carbon supported Mo–K catalysts take superiority to that over alumina in alcohol synthesis, just as revealed in Table 3. So, the sulfided Mo–K/AC catalysts in this work are expected good performance at appropriate reaction conditions.

4.2. *Comparison of Surface Interaction with Mo–K Catalysts over Alumnia Support*

It is interesting to compare the structure of Mo–K/AC catalysts with those reported for the Mo–K/Al_2O_3 system. In the case of alumina, there is a strong interaction between molybdenum species and support; and Mo mainly exists in the form of K–Mo–O species and its intensity of diffraction peaks increase with Mo loading; no MoO_2 or MoO_3 phase could be detected on oxidic samples. Moreover, $Al_2(MoO_4)_3$ phase is also formed at high preparation temperature (21). There is consensus that in the oxidic precursor, up to higher surface loadings (24 wt%MoO_3), Mo is dispersed on the alumina surface as a monolayer of (poly-) ions (22). This is in contrast to the Mo–K/AC system where small three-dimensional particles are present. The results of XRD and LRS show that, in the oxidic state, the Mo phase on samples with low Mo loading (below 24 wt%MoO_3) is mainly present as MoO_2 and in the form of $K_2Mo_2O_7$ species at higher Mo loading (up to 72 wt% MoO_3). When compared with the alumina support, the interaction between activated carbon and molybdenum phase is much weaker.

During sulfiding some aggregation of the active phase takes place (as shown in Table 1), even at the low Mo loading where small three-dimensional sulfide particles are formed on the activated carbon support. Clearly, this observation points to a certain mobility of the Mo phase during sulfidation, indicating that no strong interactions between the active phase and the support (as encountered for the alumina-supported systems) are present, even at low Mo surface loading. Most of the aggregation probably takes place during the actual sulfiding (O for S substitution) of the catalysts. The sulfidation process of the Mo–K/AC catalyst can be described by analogy to the sulfidation of Mo–K/Al_2O_3 catalyst (10). Low-temperature sulfiding occurs through simple O–S substitution reactions on the Mo(VI) ion, viz., $Mo(VI)–O^{2-} + H_2S \rightarrow Mo(VI)–S^{2-} + H_2O$. Reduction of Mo(VI) to Mo(IV) takes place through the rupturing of Mo(VI)–sulfur bonds and the formation of elemental sulfur. The elemental sulfur produced adsorbs on the support surface and is reduced with H_2 to H_2S at 510 K.

It becomes clear from these results, due to differences in the interaction between the MoS_2 phase and the support surface, that on alumina a large slab monolayer is strongly interacting with the support (17), whereas on carbon the small three-dimensional particles are essentially free of interaction with the support. The question remains as to how to explain the difference in alcohol synthesis activity observed for these two Mo sulfide phase on the basis of their different configurations. Or stated differently, how can one understand that the interaction with the alumina support lowers the alcohol synthesis activity of deposited Mo sulfide? Candia *et al.* (23) suggested that the Mo edge atoms may be bound preferentially to the alumina support by oxygen–metal linkages, due to the more reactive nature of the Mo edge plane compared to basal plane atoms. This strong bonding is not favorable for creating more active sites for CO hydrogenation.

4.3. *Influence of Surface Acidity*

On the other hand, the surface of γ-alumina is rich of acidic site (24), while activated carbon is neutral in this respect. It is well known that the acid sites on the γ-alumina surface were demonstrated to be the active sites for alcohol dehydration. So, a part of the alcohol formed during the reaction is decomposed immediately at the surface, i.e., the acidity of the γ-alumina surface greatly decreases activity of alcohol synthesis. According to our previous research, the STY and selectivity of mixed alcohol decrease monotonically with the increase in acidity of Mo–K/Al_2O_3 catalysts. Acidic support is not suitable for alcohol synthesis (24). Avlia *et al.* also reported that for Mo–K based catalyst on different supports such as $ZnCr_2O_4$, ZrO_2, Cr_2O_3, and ZnO, the selectivity to mixed alcohols varied and increased in the order $ZrO_2 < ZnCr_2O_4 < Cr_2O_3 < ZnO$; the decrease of the decrease of the acidity of the surfaces was in the some order (25).

Based on the foregoing finding, it may be argued that it is possible to increase the alcohol formation activity of alumina-supported catalysts by eliminating or reducing the strong acidity. It may be accomplished by increasing the calcining temperature such that the H–O–Al bonds responsible for the interaction are broken. This has been studied by Fu *et al.* (26) for Mo–K/Al_2O_3 catalysts. They observed that the recalcination process of the oxidized precursors is important for alcohol synthesis. Structural studies indicated that after recalcination at a high temperature of 1073 K, the BET surface area of the samples drastically decreased and Mo–K interaction species were aggregated. However, the amount of acidic sites decreased, and both the yields and the selectivity to mixed alcohol were sharply enhanced (24).

It is clear from the above discussion that the acidic surface of alumina has a negative effect on the alcohol synthesis activity of the deposited Mo sulfide. Because of the absence of such acidity when using carbon as a support, higher alcohol formation activities are obtained for Mo–K/AC catalysts compared with Mo–K/Al_2O_3 samples even when the oxidized precursors were calcined at high temperature.

5. CONCLUSION

In oxidic state, the Mo phase on the sample with low Mo loading is mainly dispersed as MoO_2, possibly because part of the potassium anions permeate into micropores of active carbon and because of the reducing nature of activated carbon at a high preparation temperature. As the Mo loading increases, the interaction between potassium and molybdenum is enhanced. At the MoO_3 loading of 72 wt%, Mo mainly exists in the form of $K_2Mo_2O_7$ species.

After sulfidation, the O–S substitution takes place, the Mo phase is highly dispersed as tiny three-dimensional particles at higher loading. XRD, LRS, and EXAFS results demonstrate that MoS_2 is the major phase present after sulfidation. The higher catalytic activity for Mo–K/AC compared to Mo–K/Al_2O_3 is explained by the difference in the structure of sulfide phase and in the interaction between these active phases and the respective supports.

ACKNOWLEDGMENTS

Thanks are due to D. M. Chen for his assistance in the LRS analysis of the sulfided catalyst samples. The provision of funds by National Natural Science Foundation of China (No. 29773042) and the use of the EXAFS experimental facility by BSRF are also gratefully acknowledged.

REFERENCES

1. Anderson, E. V., *Chem. Eng. News.* **14**, 18 (Apr. 1986).
2. Koizumi, N., Kobayashi, Y., Ozaki, O., Murai, K., and Yamada, M., *Abstr. Pap.-Am. Chem. Soc.* **218**, 19 (1999).
3. Cochran, G. A., Murchison, Craig, B., Quarderer, G. J., and Stevens, R. R., U.S. Patent 4,825,013 (1989).
4. Stevens, R. R., U.S. Patent 4,882,360 (1989).
5. Cochran, G. A., and Quarderer, G. J., U.S. Patent 4,749,724 (1988).
6. Conway, M. M., Murchison, C. B., and Stevens, R. R., U.S. Patent 4,675,344 (1987).
7. Li, X. G., Feng, L. J., Liu, Z. Y., Zhong, B., Dadyburjor, D. B., and Kugler, E. L., *Ind. Eng. Chem. Res.* **37**(10), 3853 (1998).
8. Duchet, J. C., van Oers, E. M., de Beer, V. H. J., and Prins, R., *J. Catal.* **80**, 386 (1983).
9. Moene, R., Tazelaar, F. W., Makkee, M., and Moulijn, J. A., *J. Catal.* **170**, 311 (1997).
10. Arnoldy, P., van den Heijkant, J. A. M., de Bok, G. D., and Moulijn, J. A., *J. Catal.* **92**, 35 (1985).
11. Vissers, J. P., Scheffer, R., Bachelier, J., ten Doeschate, H. J. M., Duchet, J. C. B., de Beer, V. H. J., and Prins, R., *in* "8th International Congress on Catalysis, Berlin, 1984," Vol. II, p. 387. Verlag Chemie, Weinbeim, 1984.
12. Sayers, D. E., and Bunker, B. A., *in* "X-Ray Absorption Principles, Applications, Techniques of EXAFS, SEXAFS and XANES," (D. C. Koningsberger and R. Prins, Eds.), p. 211. Wiley, New York, 1988.
13. Lu, W., Fu, Y., Xu, C., Huang, Z., Wu, J., and Fan, C., *Chinese J. Chem. Phys.* **2**, 222 (1989).
14. Williams, C. C., and Ekerdt, J. G., *et. al., J. Phys. Chem.* **95**, 8781 (1991).
15. Schader, G. L., and Cheng, C. P., *J. Catal.* **80**, 369 (1983).
16. Stern, E., Newville, M., Ravel, B., Yacoby, Y., and Haskel, D., *Physica B* **208/209**, 117 (1995).
17. Li, Z. R., Fu, Y. L., and Jiang, M., *Appl. Catal. A* **187**, 187 (1999).
18. Bridgewater, A. J., Burch, R., and Mitchell, P. C. H., *J. Catal.* **78**, 116 (1982).
19. Oades, R. D., Morris, S. R., and Moyes, R. B., *Calat. Today* **7**, 199 (1990).
20. Bian, G. Z., Fu, Y. L., and Yamada, M., *Appl. Catal. A* **144**, 79 (1996).
21. Jiang, M., Bian, G. Z., and Fu, Y. L., *J. Catal.* **146**, 144 (1994).
22. Wang, L., and Hall, W. K., *J. Catal.* **77**, 232 (1982).
23. Candia, R., Sorensen, O., Villadsen, J., Topsøe, N. Y., Clausen, B. S., and Topsøe, H., *Bull. Soc. Chim. Belg.* **93**, 763 (1984).
24. Bian, G., Fan, L., Fu, Y., and Fujimoto, K., *Ind. Eng. Chem. Res.* **37**(5), 1736 (1998).
25. Avila, Y., Kappenstein, C., Pronier, S., and Barrault, J., *Appl. Catal. A* **132**, 97 (1995).
26. Fu, Y. L., Fujimoto, K., Lin, P. Y., Omata, K., and Yu, Y. S., *Appl. Catal. A*. **126**, 273 (1995).